**Scholars Journal of Physics, Mathematics and Statistics** OPEN ACCESS
Abbreviated Key Title: Sch J Phys Math Stat
ISSN 2393-8056 (Print) | ISSN 2393-8064 (Online)
Journal homepage: https://saspublishers.com

# Synthesis, Study the Triclinic Crystal Structure, Phase Width and Morphology Performances of A Novel G-Brass Type Phases in Ternary Intermetallc Alloy Bi-La-Sn System Via Powder XRD

Rohit K. Dev[1], Hareram Mishra[2], Janak Adhikari[1], Parashuram Mishra[1*]

[1]Bioinorganic and Materials Chemistry Research Lab. M. M. A. M. Campus, Biratnagar, Nepal
[2]Department of Physics, R. R. M. Campus, Janakpurdham, Nepal

**DOI:** 10.36347/sjpms.2020.v07i12.005 | **Received:** 03.12.2020 | **Accepted:** 15.12.2020 | **Published:** 21.12.2020

***Corresponding author:** Parashuram Mishra

**Abstract** **Original Research Article**

In this research, Bi-La-Sn ternary phases were synthesized by high-temperature solid-state synthesis. Structural characterization was performed by means of X-ray diffraction and energy dispersive X-ray analysis. The ternary compounds were found to adopt g-brass (Cu5Zn8) structure type. X-ray diffraction analyses show that g-brass type phases in Bi-La-Sn system crystallize in triclinic crystal system having space group P-1. Ternary Bi-La-Sn g-brass type phases exist in an extended homogeneity range. The phase-pure ternary compounds are found to exist for compositions ranging between 50 and 60 atomic % Bi, between 10 and 40 atomic % La, and between 5 and 20 atomic % Sn. The phase width arises due to the statistical distribution of constituent elements, which is typical for intermetallic compounds. The Bi-La-Sn g-brass structures consist of two compositionally different g-clusters (consists of the four polyhedral shells: inner tetrahedron (IT), outer tetrahedron (OT), octahedron (OH), cuboctahedron (CO)) centered at high symmetric sites in a primitive triclinic unit cell. The g-brass cluster (A) at (0,0,0) site is Bi-rich, chemically more ordered than the cluster (B) present at (½,½,½). For A cluster, only IT site is mixed (La/Sn) and OT, OH, CO sites are exclusively occupied by Bi, throughout the entire homogeneity range. The B cluster is heavily disordered; only the OT site is exclusively occupied by Bi all over the phase region. For La rich region IT site is fully occupied by Sn, then mixed occupied between Bi and Sn at intermediate Sn-concentration, and completely occupied by Bi at Bi-rich side of the Bi-La-Sn phases. OH site is fully occupied by Sn at Sn rich side. The same site is mixed occupied between Bi, La and Sn for the composition at intermediate La-concentration and La/Sn at Bi poor side. CO site of B cluster is occupied by La and Sn. The electrochemical properties of four Bi-La-Sn based samples with different compositions were studied as an anode material for lithium and sodium-ion storage using galvanostatic charge-discharge cycles. Li-ion half-cells transpired excellent retention of charge capacity (>80%) with more than 99% Coulombic efficiency. The results further encourage the prospects of ternary Bi-La-Sn alloy anodes to utilize in real energy storage applications Therefore, we investigated the phase relations of and crystal structure this system experimentally by powder XRD method using ab ignition methods, in order to understand the lithiation pathways during charge and discharge process. The samples were further characterised using several physicochemical methods to reveal their morphology, structure, chemical and electrochemical properties. X-ray diffraction confirms the Bi-La-Sn alloy formation on the graphitic support and energy dispersive X-ray spectroscopy highlights the presence of the three metallic components from the alloy structure. As a consequence of the process of synthesis, the crystal size refinement was observed in all cases, meanwhile, the particle size increased due to the powders ductility.

**Keywords:** Intermetallic; ternary; intermediate; octahedron; polyhedral; cell.



## INTRODUCTION

As early as in the beginning 20th century [1905Gui] and [1906Gui] performed systematic studies of replacing Zn by Al, Fe, Mg, Mn, P, Pb, Sb, Si and Sn in a number of Cu-Zn brasses. They determined the volume fraction of the alloy and (phases in Cu-Zn alloys and their mechanical properties with the addition of these alloying elements). Comparable systematic studies were made by replacing Zn by Al, Fe, Ni and Sn in Cu-Zn brasses [1]. Similar alloy development studies, regarding the effect of Si and Sb on the microstructure of Al-Cu-Zn bronzes. All these laborious alloy development studies were performed by carefully examining the microstructure and determining the mechanical properties. Al-Cu-Zn alloys exhibit high

damping capacity, shape memory effects and super elasticity which allows a wide variety of possible use.The goal is to be accomplished by implementing a solid and reliable energy matrix, pointing to achieve a target of a net zero $CO_2$ emission by 2050 [2]. This difficult task for the energy sector requires additional strategies in order to achieve the desired values. Among solar, biomass and wind power, hydrogen, regarded as an energy vector, has a real potential of progress for the next decades. Currently, hydrogen-based energy covers only a minor part from the total energy consumption [3]. Hydrogen can be directly converted into electricity, when applied in fuel cells, exhibiting high current efficiencies [4]. Considered an emerging alternative to the widely employed fossil fuels, it can be obtained from numerous sources by applying diverse methods (steam reforming, coal gasification, or water electrolysis) [5]. Currently, 96% from the total hydrogen production is covered from fossil fuels, being associated with significant CO2 emissions. Among all the accessible strategies for hydrogen production, electrochemical water splitting represents the most promising approach. It is described as a less environmentally harmful process, with "zero" emissions, if the necessary electrical energy is generated from CO2-free and renewable sources [6]. Accordingly, the hydrogen evolution reaction (HER) is currently the most studied electrochemical reaction [7]. Proton exchange membrane (PEM) electrolysers deliver a promising alternative to an efficient hydrogen production, as they provide numerous advantages over the other techniques, such as significant current densities at high system efficiency [8-10]. Experts are confident that PEM electrolysis cells will be the leading water splitting technology by 2030, especially due to superior characteristics during intermittent operation [11]. The current state-of-the-art mentions Bi-La-Sn. La black and carbon supported Sn nanoparticles as efficient catalysts, for cathodes in PEM electrolysers [12], as for the anodes, they consist mainly in more corrosion resistant materials, like Ir, IrO2 or Ru and RuO2, either supported or unsupported[13]. Even so, the scarcity and high price of the noble metals brings limitations and transforms this technology in a very expensive one. Highly dispersed platinum supported catalysts are usually materials of choice for HER in PEM electrolysers [14]. A further lowering of the platinum amount is strongly required in order to meet the economic targets. Non-noble metal chalcogenides based catalysts such as MoS2 [15,16] or CdS [17] have been recently investigated regarding their activity towards the hydrogen evolution reaction, either in acidic or alkaline media. Another available alternative, which is currently explored, consists in alloying platinum with transition metals like Co Ni Mn [18], leading in this way also to a significant improvement of the activity and stability. Several studies have reported that platinum alloyed with two or more transition metals exhibits superior performance. The main features when choosing catalyst materials are the catalytic activity, high electrical conductivity and corrosion resistance in the working conditions [19, 20]. Transition metal alloys have been proven to exhibit significant electrocatalytic properties towards hydrogen evolution reaction, both in acid and alkaline aqueous solutions. The possibility to develop ternary Bi-La-Sn alloys for catalytic applications has been endeavourer in several studies, especially as cathodes for PEM fuel cells [21],. Currently, there are limited methods that fit this purpose, such as chemical or sputtering all of them being complicated, time consuming and cost-intensive. The electrochemical method represents an appealing alternative for depositing a ternary alloy, due to its facile application and short deposition time in comparison with other techniques. A major limitation in platinum-transition metals ternary alloys electrode position may arise from the difficulty of co-depositing the noble metal species simultaneous with the less noble ones. The catalytic activity depends mainly on the electronic structure of the material and moreover, alloying various metals often leads to a significant increase in the activity of the final compound. Bi-La-Sn is an electro catalytic reaction that mainly depends on the adsorption energy of atomic hydrogen. Typical volcano plots display the relationship between the catalytic activity of the metals and their Gibbs free energy (DGH) for hydrogen adsorption. A catalyst having DGH value near zero exhibits the best electro catalytic activity for hydrogen [22]. For the most active metals, a fast deactivation is often observed due to adsorption or electrodeposition of impurities. Improvements in preparation technique and very clean surfaces and solutions, lead to catalysts with higher activities . Regarding alloys and intermetallic compounds, a maximum in bond strength and stability is expected when metals located on the left half of the transition group, which possess empty or half and full vacant of d-f –orbital's of cited metals vacant d-f orbitals, are alloyed with metals situated on the right half of the transition main group metal ion as Bi which are good malleable with other metal ions group, having internally paired d-electrons, not available for bonding in pure metals .This may be the reason why Bi alloyed with La and Sn can provide superior catalytic activity compared to conventional La/ C electrodes. . Moreover, the literature was limited to the specific characteristics of compounds with a lack of valid crystallographic data. Motivated by the previously reported Cu6-xZn2þxSb2 ($0 \leq x \leq 1.0$), it was attempted to uncover the existence of Cu-Zn-Sn ternary phases starting from Cu6-xZn2þxSn2. It is noted that in Zr-Ni binary system, Cu41Sn11 (cF416; F43m; 216) is the only compound reported in the phase diagram that bears a close resemblance to g-brass type phase [23]. The main objectives of the present study are to explore the structure, chemical compositions, and phase width of g-brass type Bi-La-Sn ternary system and electrochemical properties of g-brass alloys in Bi-La-Sn system in rechargeable Li and Na-ion batteries. Thermodynamic data for the Li-Sb-Sn system are available from Berger

and Flandorfer, who determined the partial and integral molar enthalpies of mixing of liquid Bi-La-Sn alloys at 801$^{o}$C [24]. They found a strong exothermic mixing behavior of the Bi-La-Sn system with a minimum of DmixHz-65 kJ mol$^{-}$1 in the binary Li-Sb system close to xLi = 0.75[25]. In the course of their work they further estimated the phase boundary of the liquid at 801$^{o}$C and showed that the primary formation of the high melting compound Bi-La-Sn dominates the solidification behavior of the entire system.This work described the synthesis and study the crystal structure of cited intermetallic alloy.

## MATERIALS AND METHODS

All the chemicals used were in this work high purity (99.99%) and purchased from Sigma Aldrich Ternary compounds in Bi-La-Sn system were synthesized by high-temperature solid-state synthesis. Highly pure La (shot, 4-6 mm, 99.999%, ), Ni (teardrop-shot, 1-5 mm, 99.999%,) and Bi (shot, 6 mm, 99.999%,) were taken inside a quartz tube (diameter of 8 mm) according to their weight calculated from the nominal composition (in 300 mg scale). Then the tube was sealed under a high vacuum (~10.5 mbar) using a sealing unit equipped with a diffusion pump. The sealed ampoule (length 3 cm) was kept in a programmable chamber furnace (At 1200$^{o}$C muffle furnace)[26]. Initially, the ampoule was heated up to 500 $^{o}$C by fast heating (120$^{o}$C/h), and the temperature dwelled for 24 h. The reaction mixture was then again heated to 850$^{o}$C with 12$^{o}$C/h ramping rate and hold at that temperature for 24 h for homogenizing the metal mixture. After that, the temperature was slowly (12$^{o}$C/h) reduced to 450$^{o}$C and annealed at that temperature for the duration of 84 h. Finally, the furnace was again cooled down to 250$^{o}$C with a ramping rate of 6$^{o}$C/h, and it was turned off to allow the ampoule for air cooling[26]. A series of samples were prepared with a varied composition of La,Sn and Bi using the previously mentioned temperature program to check the phase purity and determine the homogeneity range. Ingots obtained were brittle in nature with a silvery metallic luster and stable in air and water at room temperature [27].

Powder X-ray diffraction (PXRD) and refinement PXRD was used for checking phase purity and phase detection. Room temperature (298 K) PXRD data were collected in a Rigaku fifth generation (Gen 5) MiniFlex600 desktop X-ray diffractometer, with the HyPix-400 MF 2D hybrid pixel array detector (HPAD) equipped with Cu Ka radiation (1.5418 Å). A Bruker D2 Phaser XRD with LYNXEYE XE-T detector was used for some PXRD experiments. All the diffraction patterns were recorded over 2θ range 20-90$^{o}$ with a step size 0.02. Rietveld refinements were carried out using JANA 2006 program[28]. 15th order Legendre polynomials were used to fit the background and the zero point error was refined freely. Reflections were fitted with the Pseudo-Voigt function (peak-shape function: GW, LX, LY; cutoff: 12 [29]. Peak asymmetry corrections were done when it was relevant. Refining the profile parameters, profile fit was achieved and to determine the phase purity of the compounds Rietveld refinement was performed. Structural properties, phase transformation and crystal structure, of the milled samples as a function of the compositions were characterized by X-ray diffraction (XRD) using an Inel Equinox 2000 diffractometer [30]. The powder diffraction patterns were collected and ranged from 5$^{o}$ to 90$^{o}$in 2θ with Cu Ka (1.56541A) radiation. Rietveld refinement was performed on the X-ray diffraction patterns using the program High score plus [31], in order to calculate the phase amount and index in Crysfire software programme to determine cell parameters. This method takes into account all the information collected in a pattern and it uses the least-squares approach to refine a theoretical line until it matches the measured profile. The crystallite size (D) and internal microstrain (ε) in the milled samples were calculated from the XRD line broadening using the Debye-Scherer formula for particle size. Morphological characterization was performed using a TESCAN MIRA 3 scanning electron microscopy (SEM).

.

## RESULTS AND DISCUSSIONS

### Structural Analysis

A powder X-ray diffraction (P-XRD) diagram of **$Bi_{1.752}$ $La_{0.123}$ $Sn_{2.312}$** is shown in Figure 1. The intense Bragg-peaks were indexed in hexagonal symmetry and the lattice parameters were determined as **a=2.8090(9) Å b=3.5882(5) Å c=6.4867(19) Å α=102.44(2)° β=92.974(15)° γ=107.290(17)°**by cell refinement. And refinement value are GOF=0.133,Rwp=3132 and Rp=0.68811.The reflections which can be assigned to small amounts of the side product **$Bi_{1.752}$ $La_{0.123}$ $Sn_{2.312}$** of the initial mixture powders in a linear scale is shown, which allows to identify the phases in the un-milled powders, since it is possible to observe that the peaks in the mixture confirm the presence of La with a phases that coexist at room temperature, Bi (tetragonalgonal close-packed) and La (face-centered cubic), furthermore, other phases corresponding to Sn (body centered cubic) were observed. Additionally, an inset is included on a square root scale to show all planes and to clarify the low-intensity peaks from the background. The results obtained from the refinement analysis in the un-milled powders, are shown in Table 1. As can be noted, the weight percentage of Bi is the majority phase concerning the Bi. So, the weight percentages of La and Sn are according to the percentages of the samples before the milling process. The phases identified of **$Bi_{1.752}$ $La_{0.123}$ $Sn_{2.312}$** It is important to highlight that the main peak of La and Sn (located at 21 of 2θ degree) are difficult to appreciate due to their overlap whit the main peak of the Bi fcc and hcp but, the next peaks and the refinement results of each phase confirm the presence of these elements, in order to analyze the results obtained from each ternary alloy, is generated the following discussion.

When the mixture $\mathbf{Bi_{1.752}\ La_{0.123}\ Sn_{2.312}}$ is subjected to 6 h of milling time, an allotropic transformation in the La structure occurs, since no peaks corresponding to Bi (tetragonal close-packed) phase are found in the composition. This phenomenon is attributed to the stabilized of the face-centered triclinic Bi phase promoted by the diffusion of the atoms of bcp-La toward fcc-Sn structure, due to the high energy generated during the milling process. This effect has already been studied by other researchers [32]. Furthermore, the X-ray diffraction confirms the formation of an a Bi-La-Sn solid solution promoted by the diffusion of theBi and Laatoms, toward the Sn structure. On the other hand, in the XRD pattern corresponding with $\mathbf{Bi_{1.752}\ La_{0.123}\ Sn_{2.312}}$ composition which is shown in the broadening of the peaks located at ~51.7$^{o}$ ~60.5$^{o}$ and ~80$^{o}$C of 2θ are observed, which indicates that a refinement promoted by the decrease in the crystal size from 40.27 nm to 20 nm occurred. Also, the above mentioned can be corroborated with the MAUD refinement (not shown here), whose values are presented in Table 1. Due to the severe plastic deformation generated by the mechanical alloying, a slight peak displacement can be observed in Rietveld refinement observation shown in figure. On the other hand, when the $\mathbf{Bi_{1.752}\ La_{0.123}\ Sn_{2.312}}$ composition was milled during 7 h, the same effect was observed, i.e., Bi-La-Sn inetrmetallic was observed. Moreover, in Figure.1 is observed a slight peak displacement, associate with the lattice parameters distortion and the broadening of the peak (1 1 1) located at ~51.9_ in 2θ degree, this phenomenon can be attributed to modifications in the crystallite size from 21.18 to 11.83 nm, and/or lattice strain which can be explained by the differences of lattice parameters between **Bi-La-Sn** is formed a solid solution. Finally, the $\mathbf{Bi_{1.752}\ La_{0.123}\ Sn_{2.312}}$ mixture is shown in Fig. 2 a) after being subjected to 7 h of milling time, and it was possible to observe only the (1 1 1) (2 0 0) and (2 2 0) planes, corresponding with fcc-structure, which indicates that a $\mathbf{Bi_{1.752}\ La_{0.123}\ Sn_{2.312}}$ solid solution, had been formed. In this case, the diffusion of the Bi and La atoms toward the Sn--phase had occurred, this argument can be corroborated with the refinement results shown in Table 1. On the other hand, in Figure - 2 shown refined graph it can be observed a slight peak displacement toward the left, which indicates an increment in the lattice parameter, attributed to the lattice parameter distortion. It's important to mention, that the ternary Bi-La-Sn phase diagram predicts the formation of a-Bi and g-La and Sn phase for the compositions $\mathbf{Bi_{1.752}\ La_{0.123}\ Sn_{2.312}}$ under equilibrium conditions. However, mechanical alloying is a non-equilibrium processing technique. The choice of the phase strongly depends on the ratio of the mole-fraction of Bi and La. Besides, the formation of a is possible to obtain depending on the milling time. As a complementary characterization to the powder XRD spectra shown in figure 1. And structural analysis, parameters such as the crystal structure, cell parameters, crystal size, particle diameter, microstrains were obtained by Rietveld refinements, which are shown in Table,2 and 3D structure is shown in figure 3.

.

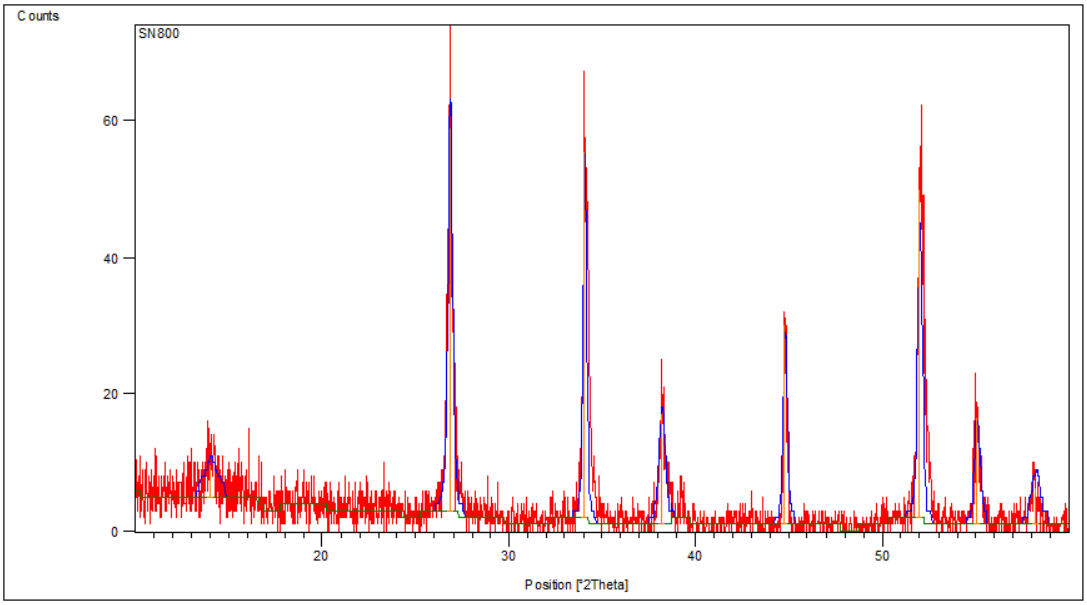


**Fig-1: Powder XRD spectra of Bi-La-Sn alloy**

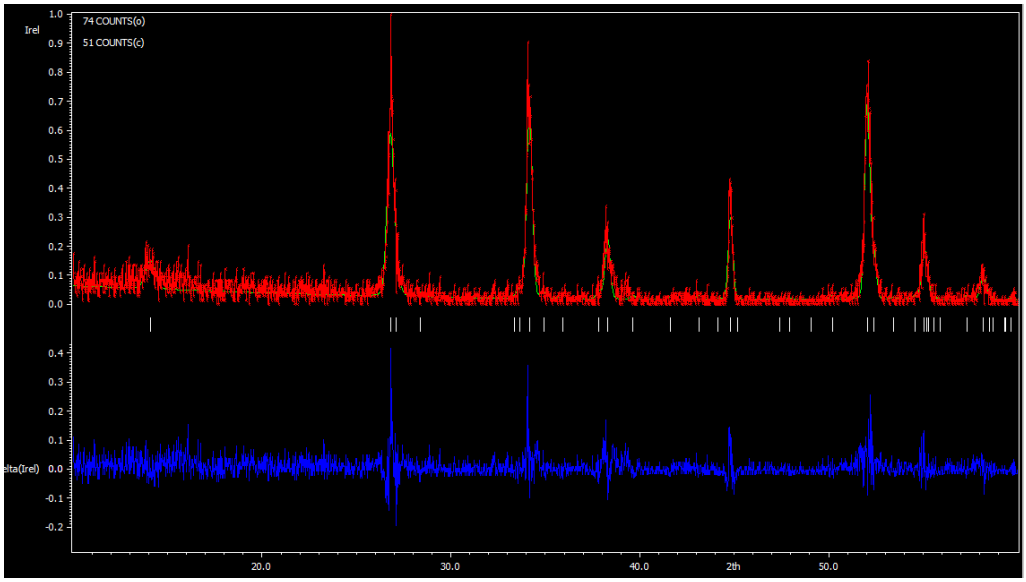


**Fig-2: Rietveld refinement graph of $Bi_{1.752}$ $La_{0.123}$ $Sn_{2.312}$**

**Table-1: Crystallographic Phase data**

| | |
|---|---|
| Formula sum | $Bi_{1.752}$ $La_{0.123}$ $Sn_{2.312}$ |
| Formula weight | 657.7 g/mol |
| Crystal system | triclinic |
| Space-group | P -1 (2) |
| Cell parameters | a=2.8090(9) Å b=3.5882(5) Å c=6.4867(19) Å α=102.44(2)° β=92.974(15)° γ=107.290(17)° |
| Cell ratio | a/b=0.7828 b/c=0.5532 c/a=2.3093 |
| Cell volume | 60.49(3) $Å^3$ |
| Z | 2 |
| Calc. density | 36.1086 $g/cm^3$ |
| Meas. density | 35.9761$g/cm^3$ |
| Pearson code | aP4 |
| Formula type | NO |
| Wyckoff sequence<br>Index<br>Refine value | Ieb<br><br>0≤h≤1,0≤k≤3,-1≤l≤2<br><br>GOF=0.133,Rwp=0.3132,Rp=6811 |

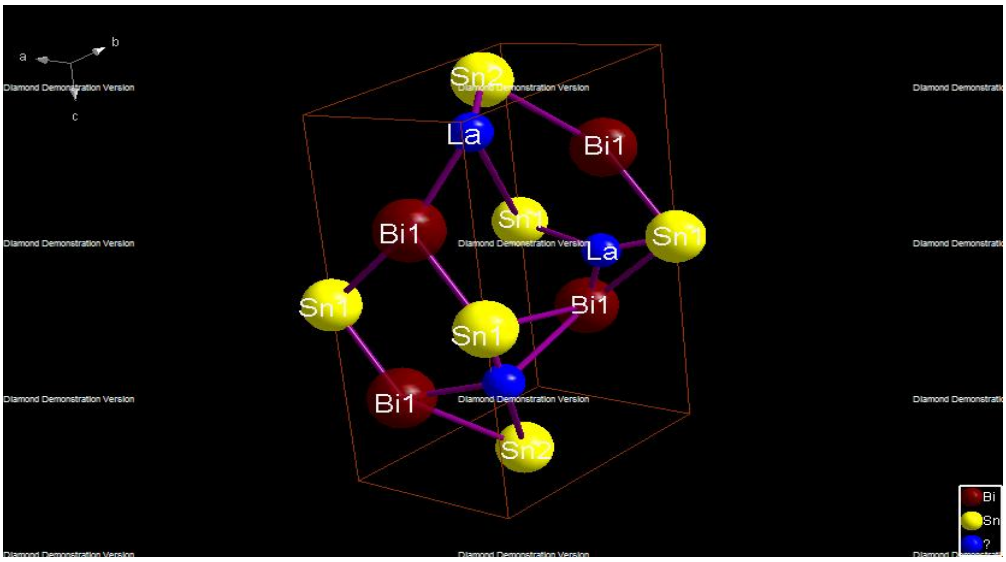


**Fig-3: 3D structure of $Bi_{1.752}$ $La_{0.123}$ $Sn_{2.312}$ obtained from CIF**

**Table-2: Fraction Atomic parameters**

| Atom | Ox. | Wyck. | Site | | x/a | y/b | z/c | U [Å$^2$] |
|---|---|---|---|---|---|---|---|---|
| Bi1 | +3 | 2i | 1 | | 0.39083 | -0.00492 | 0.27160 | |
| Sn1 | +2 | 1b | -1 | | 0 | 0 | 1/2 | |
| Sn2 | +4 | 1e | -1 | | 1/2 | -1/2 | 0 | |
| La | +3 | 2i | 1 | | 0.31200 | 0.06712 | 0.08712 | |
| La | +3 | 2i | 1 | | 0.00000 | 0.05412 | 0.65130 | |
| La | +3 | 2i | 1 | | 0.07412 | 0.09654 | 0.04368 | |
| Bi | +3 | 2i | 1 | | 0.32170 | 0.87130 | 0.52340 | |

**Table-3: Selected bond angles**

| | | | |
|---|---|---|---|
| Bi1 | La | La | 107.156 |
| | La | Sn1 | 25.870 |
| | La | Sn1 | 110.929 |
| | La1 | Sn1 | 129.730 |
| | La2 | Sn2 | 69.015 |
| Sn1 | La1 | La | 180.000 |
| Sn | La2 | Bi1 | 55.085 |
| La | Bi1 | Sn2 | 146.549 |
| | La | Bi1 | 112.932 |
| Sn2 | La | La | 180.000 |
| | La | Bi1 | 99.672 |
| La | La | La | 36.504 |
| | La | Bi1 | 125.375 |
| | La | La | 117.906 |
| | La | Sn2 | 73.980 |
| Bi | Sn1 | La | 0.000 |
| | La | Bi1 | 83.730 |
| | La | Bi1 | 111.895 |

**SEM Micrograph**

SEM micrographs of the un-milled powders and powders milled during 7 h for $\mathbf{Bi_{1.752}\ La_{0.123}\ Sn_{2.312}}$ compositions, are shown in Figure 4. The morphology and size of the un-milled powders are shown in figure4. Bi powder has an elongated ligament-like morphology with a particle size around 20 mm, meanwhile iron powder has irregular morphology with a particle size over 80 mm and La powder has a flake-like morphology with a particle size around of 28 mm. Before the mechanical alloying process, the mixture is showed in the figure 4 where the particle diameter compositions were 75.47 mm.. After 7 h of milling [33]. As can be observed, due to the process of mechanical alloying, a noticeable change in the shape and size of the powders had occurred.

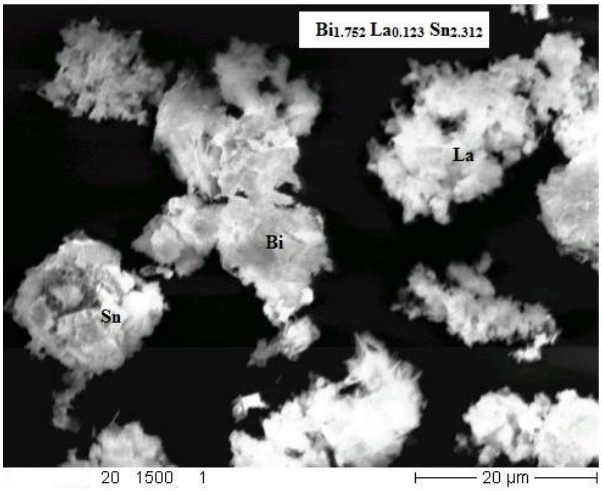


**Fig-4: SEM micrograph of $\mathbf{Bi_{1.752}\ La_{0.123}\ Sn_{2.312}}$**

As per microstructure formation during ball milling is governed by a competition between the cold welding and fracturing of powder particles under the repetitive events of impact. In these ternary alloys, the milled compositions show an irregular morphology with particle sizes around 75.5 mm according to the particle size crystallographic data shown in Table 1. Moreover, it is possible to observe that the content of the ductile elements (Bi and Sn) promotes the formation of large agglomerates when are mixed with brittle elements (La) as a result of the process of mechanical alloying.

## CONCLUSIONS

In the ternary system Bi-La-Sn only one ternary compound occurs, $\mathbf{Bi_{1.752}\ La_{0.123}\ Sn_{2.312}}$which was found in both isothermal sections. In general, both isothermal sections are similar in their general outline and actually, only differ by the variation of the binary systems with temperature. Our results show that lithiation of the binary phase $\mathbf{Bi_{1.752}\ La_{0.123}\ Sn_{2.312}}$ starts with an alloying reaction (up to40 at.% Bi at 400$^{o}$C), without changing the corresponding crystal structure.The structural analysis showed the formation of the solids solution with a triclinic phase, i.e., an fcc phase it was obtained, in all cases. As a consequence of the milling process, the crystallite size decreased in each of the compositions. SEM images showed the formation of big agglomerates promoted by cold welding and the ductile powders. On the other hand, the saturation magnetization (MS) increased with the obtaining of the solids solutions\ Since the solubility of Li seems to be retrograde, it can be expected that it exists also at ambient temperature. Further lithiation leads to a conversion reaction with the formation of Bi-La-Sn and simultaneous precipitation of small (Sn)-crystals. Ductile, micro-structured (Sn) acts as a "buffer" for mechanical stress caused by the formation of various Bi-La and La-Sn compounds. Only upon a Sn concentration of approx. 60 at.% also La-Sn alloys start to form by litigation . Our investigations were performed on alloys annealed at 300 $^{o}$C and 600$^{o}$C, although knowledge of phase relations at lower temperatures, at whichLa-Sn usually operate is crucial. It has to be noted that phase equilibria at room temperature are not experimentally accessible by liquid alloying at high temperatures. This especially applies to Bi-La-Sn where primary crystallization of is Figure 4 SEM micrograph of $\mathbf{Bi_{1.752}\ La_{0.123}\ Sn_{2.312}}$ dominant. Nevertheless, a reliable extrapolation to ambient temperature is possible In this way the prediction of the reaction pathway during the lithiation at room temperature using Sb/Sn as anode material would be possible. Future large scale applications of Bi-La-Sn anodes in galvanic cells are limited by relatively high costs of the materials and the discussion of declaring Sn as a highly applicable material which has to be largely production from industrial productions so this intermettalic alloy can be applied huge amount in future the they are still interesting as niche products for special applications can be used in nanomaterials as super conductor materials.

**Declaration of Competing Interest**

All authors each made a significant contribution to the research reported and have read and approved the submitted manuscript. At the same time, the authors declare that they have no conflict of interests or personal relationships that could have appeared to influence the work reported in this paper.

## ACKNOWLEDGMENTS

The authors would like to acknowledge the immense contribution laboratory staff of Department of Chemistry University of Delhi,India for provide the XRD data.

## REFERENCES

1. Reddy GS, Sahu SR, Prakash R, Jagannatham M. Synthesis of cobalt-rich alloys with high saturation magnetization: a novel synthetic approach by hydrazine reduction method. Results Phys 2019;12:652-61.
2. Chitsazan B, Shokrollahi H, Behvandi A, Ghaffari M. Magnetic, structural and microstructural properties of mechanically alloyed nano-structured Fe48Co48V4 powder containing inter-metallic Co3V. J Magn Magn Mater 2011;323:1128-33.
3. Baghbaderani HA, Sharafi S, Chermahini MD. Investigation of nanostructure formation mechanism and magnetic properties in Fe45Co45Ni10 system synthesized by mechanical alloying. Powder Technol 2012;230:2416.
4. Betancourt-Cantera JA, S_anchez-De Jesu´ s F, Boları´n-Mir_o AM, Torres-Villase~nor G, Betancourt-Cantera LG. Magnetic properties and crystal structure of elemental cobalt powder modified by high-energy ball milling. J. Mater. Res. Technol. 2019;8(5):4995e5003.
5. Betancourt-Cantera JA, Boları´n-Mir. AM, S_anchez-De Jesu´ s F, Betancourt-Cantera LG, Crystal structure and magnetic properties of Co-Mo alloys produced by mechanical alloying. Jpn Mag 2020;25(1):36-42.
6. Bolokang AS, Phasha MJ, Camagu ST, Motaung DE, Bhero S.Effect of thermal treatment on mechanically milled cobalt powder. Int J Refract Met Hard Mater 2010;31:258-62.
7. Ramı´rez-Meneses E, Torres-Huerta AM, Domı´nguez-Crespo MA, Ponce-Varela MG, Hern_andez-P_erez MA, Betancourt I, et al. Synthesis and electrochemical characterization of Ni nanoparticles by hydrazine reduction using hydroxyethyl cellulose as capping agent. Electrochim Acta 2014;127:228-38.

8. Paganotti A, Bessa CVX, Ferreira LDR, Gama S, Silva RAG. Annealing effect on thermal, mechanical and magnetic properties of Fe-Ni-Co alloys. J Alloys Compd 2019;811:152029.
9. Osaka T. Electrodeposition of highly functional thin films for magnetic recording devices of the next century. Electrochim Acta 2000;45:3311-21.
10. Raanaei H, Eskandari H, Mohammad-Hosseini V. Structural and magnetic properties of nanocrystalline Fe-Co-Ni alloy processed by mechanical alloying. J Magn Magn Mater 2016;398:190-5.
11. Prasad NK, Kumar V. Microstructure and magnetic properties of equiatomic FeNiCo alloy synthesized by mechanical alloying. J Mater Sci: Mater Electron 2015;26:10109-18.
12. Pikula T. Correlations between hyperfine magnetic field and some macroscopic magnetic quantities in mechanosynthesized CoxFeyNiz alloys. Nukleonika 2013;58(1):153-167.
13. Bahgat M, Min-Kyu Paek, Jong-Jin Pak. Comparative synthesize of nanocrystalline FeeNi and Fe-Ni-Co alloys during hydrogen reduction of NixCo1_xFe2O4. J Alloys Compd 2008;466(1-2):59-66.
14. Azizi A, Yoozbashizadeh H, Sadrnezhaad SK. Effect of hydrogen reduction on microstructure and magnetic properties of mechanochemically synthesized Fee16.5Nie16.5Co nano-powder. J Magn Magn Mater 2009;321:2729-2732.
15. Li X, Takahashi S. Synthesis and magnetic properties of FeeCoeNi nanoparticles by hydrogen plasma-metal reaction. J Magn Magn Mater 2000;214:195-203.
16. Dalavia SB, Theerthagiria J, Rajab MM, Panda RN. Synthesis, characterization and magnetic properties of nanocrystalline FexNi80_xCo20 ternary alloys. J Magn Magn Mater 2013; 344:30-34.
17. Toparli C, Ebin B, Gu¨ rmen S. Synthesis, structural and magnetic characterization of soft magnetic nanocrystalline ternary FeNiCo particles. J Magn Magn Mater 2017;423:133-9.
18. [Jiles D. Introduction to magnetism and magnetic materials. London: Chapman & Hall; 1991. p. 280-297.
19. Shafi K, Gedanken A, Prozorov R, Revesz A, Lendvai J. Preparation and magnetic properties of nanosized amorphous ternary FeeNieCo alloy powders. J Mater Res 2000;15(2):332-337.
20. Rathi A, Meka VM, Jayaraman TV. Synthesis of nanocrystalline equiatomic nickel-cobalt-iron alloy powders by mechanical alloying and their structural and magnetic characterization. J Magn Magn Mater 2019;469:467-482.
21. Yuv Raj Sahu, Parashuram Mishra, Morphology and Study the Crystal Chemistry of a Novel Ternary Mixed Valence Bi1.52 Co2.52 Zr0.751 N0.641 O8.12 Oxide Orthorhomic Crystal Structure by *Ab Initio* Method via Powder XRD, Scholars International Journal of Chemistry and Material Sciences, 2020; 3(7): 99-108.
22. M. Nespolo, A. Sato, T. Osawa, H. Ohashi, Synthesis, crystal structure and charge distribution of InGaZnO4. X-ray diffraction study of 20kb single crystal and 50kb twin by reticular merohedry, Cryst. Res. Technol. 35 ,2000, 151–165.
23. W. Assenmacher, G. Schnakenburg, Y. Michiue, Y. Kanke, N. Kimizuka, W. Mader, Synthesis and crystal structure characterization of InGaZnO4 with a new defect structure, J. Solid State Chem. 215 ,2014, 176–183.
24. N. Kimizuka, A. Takenaka, Y. Sasada, T. Katsura, New compounds Yb2Fe3O7 and Lu2Fe3O7, Solid State Commun. 15 ,1974, 1199–1201.
25. R. Grajczyk, M.A. Subramanian., Structure-property relationships of YbFe2O4- and Yb2Fe3O7-type layered oxides: A bid´s eyes view, Progress in Solid State Chem. 43 (2015) 37-46.
26. N. Kimizuka, *Private Communication*, National Institute for Research in Inorganic Materials, Ibaraki-ken, Japan, 1986.
27. G. M. Sheldrick, "SHELX-97 (Includes SHELXS97, SHELXL97, CIFTAB) Programs for Crystal Structure Analysis (Release 97-2)", University of Göttingen, 1998.
28. Parashuram Mishra, AB Initio Structure Determination of Bi0.5 Mn0.125 Mo0.5 O0.67 U0.32 Mixed Valency From Quartenary of Bi2O3-V2O5 - UO2- Mn2 O2- MoO4, International Refereed Journal of Engineering and Science (IRJES) ISSN (Online) 2319-183X, (Print) 2319-1821 Volume 9, Issue 3 , 2020, PP. 18-24.
29. S. B. Narendranath, A. K. Yadav, T.G. Ajithkumar, D. Bhattacharyya, S. N. Jha, K. K. Dey, T. Raja, R. N. Devi, Investigations into variations in local cationic environment in layered oxide series InGaO3(ZnO)*m* (*m* = 1–4), *Dalton Trans.43* ,2014, 2120-2126.
30. Y. Tanaka, K. Wada, Y. Kobayashi, T. Fujii, S. J. Denholme, R. Sekine, N. Kase, N. Kimizuka, N. Miyakwa, Singal crystal growth of bulk InGaZnO4 and analysis of its intrinsic transport properties, *Cryst. Eng. Comm.* 2019,3,241-255.